Scientific Research Publishing

Advances in Chemical Engineering and Science, 2020, 10, 378-398
https://www.scirp.org/journal/aces
ISSN Online: 2160-0406
ISSN Print: 2160-0392

Synthesis and Evaluation of Corrosion Inhibiting Activity of New Molecular Hybrids Containing the Morpholine, 1,4-Naphthoquinone, 7-Chloroquinoline and 1,3,5-Triazine Cores

Regina Westphal[1], Jorge Welton de Souza Pina[1], Juliana Panceri Franco[2], Josimar Ribeiro[2], Maicon Delarmelina[3,4], Rodolfo Goetze Fiorot[3], José Walkimar de Mesquita Carneiro[3], Sandro José Greco[1*]

[1]Laboratório de Síntese Orgânica Aplicada, Departamento de Química, Universidade Federal do Espírito Santo, Vitória, Brasil
[2]Laboratório de Pesquisa e Desenvolvimento em Eletroquímica, Departamento de Química, Universidade Federal do Espírito Santo, Vitória, Brasil
[3]Laboratório de Química Computacional, Instituto de Química, Universidade Federal Fluminense, Niterói, Brasil
[4]Today at School of Chemistry, Cardiff University, Cardiff, United Kingdom
Email: *grecosj@outlook.com

How to cite this paper: Westphal, R., de Souza Pina, J.W., Franco, J.P., Ribeiro, J., Delarmelina, M., Fiorot, R.G., de Mesquita Carneiro, J.W. and Greco, S.J. (2020) Synthesis and Evaluation of Corrosion Inhibiting Activity of New Molecular Hybrids Containing the Morpholine, 1,4-Naphthoquinone, 7-Chloroquinoline and 1,3,5-Triazine Cores. *Advances in Chemical Engineering and Science*, **10**, 378-398.
https://doi.org/10.4236/aces.2020.104024

Received: August 3, 2020
Accepted: September 19, 2020
Published: September 22, 2020

Abstract

Three molecules containing morpholine, 1,4-naphthoquinone, 7-chloroquinoline and 1,3,5-triazine cores, scaffolds with recognized anti-corrosive activity, were synthesized and had their anticorrosive activity evaluated through potentiodynamic polarization and electrochemical impedance studies. Both studies were conducted in a simulated production water medium containing 150,000 $mg{\cdot}L^{-1}$ Cl^{-} and 5 $mg{\cdot}L^{-1}$ S^{2-}. Corrosion inhibition efficiency ranged from 67% - 86%, amongst which the naphthoquinone-containing derivative (compound **1**) was the most effective. These compounds act through formation of a protective film on the surface of AISI 316 stainless steel. Investigation of the molecular properties of the prepared inhibitors by DFT calculations revealed that the LUMO energy and chemical hardness of the molecules can be directly correlated with their inhibition efficiency.

Keywords

Corrosion, Density Functional Calculations, Eletrochemical Impedance Spectroscopy, Heterocycles, Polarization

1. Introduction

The 1,4-naphthoquinone (1,4-NQ) core is a frequent unit in natural products. For decades, these substances have been used for various purposes in different application areas, from biological and medicinal [1] [2] [3] [4] to materials science [5] [6] [7]. The 1,4-NQs are highly reactive building blocks in a large variety of chemical reactions, attracting many synthetic chemists inspired by the nature to produce technologically appealing and bioactive compounds [8] [9] [10]. Quinoline (aza-naphthalene) is other scaffold presenting a similar profile with remarkable synthetic versatility and a large set of usages [11] [12]. Many synthetic and natural products bearing this unit display diverse activities, mostly biological and pharmacological [13] [14] [15].

The 1,3,5-triazine (s-triazine) scaffold, on the other hand, is not common in natural products [16]. Usually, cyanuric chloride, which is prepared by the reaction of chlorine with hydrocyanic acid under direct sunlight [17], is used as starting material to insert this skeleton into a desired compound. Given its efficient reactivity towards a range of nucleophiles, commercial accessibility, low cost, and ease of stepwise chemoselective substitutions of the three chlorine atoms [18] [19], it is frequently applied to build elaborated molecular architectures [20]. Its derivatives have been subjected to extensive studies, presenting useful agricultural and medicinal applications [21] [22]. However, some solubility-related problems are common in triazine derivatives, affecting synthesis, characterization, and application steps. To increase its derivatives solubility, the insertion of morpholine group in the triazine core has shown to be a good strategy [23] [24].

All these scaffolds exhibit the structural similarity of being planar, having conjugated π-system and heteroatoms with electron lone pair. Particularly, these are important features in the design of new organic corrosion inhibitors [25] [26] [27] [28]. A high degree of planarity enables them to adhere to the metallic surface, creating a thin protective film that avoids or decreases reactions that trigger corrosive processes [25]. Regarding the nature of anticorrosive agents, use of organic compounds as corrosion inhibitors is one of the most profitable, effective and ease methods because of their simplicity and cost-effective synthesis, using commercially available inexpensive starting materials [25]. Usually the organic inhibitors contain unsaturations in their chemical structure and/or polar groups with atoms of nitrogen, sulfur and oxygen, capable of transferring electrons to the metal, forming a strong covalent bond. Thus, metals act as electrophiles, while organic inhibitors act as nucleophiles [26] [29].

Several works reported natural and synthetic compounds bearing these cores as corrosion inhibitors. 1,4-naphthoquinone, for example, was shown to be an efficient corrosion inhibitor in aluminum in a 0.50 $mol \cdot L^{-1}$ solution of sodium chloride [30]. Compounds containing a quinoline core also showed anticorrosive activity in iron and steel in acidic solution [31] [32] [33]. Similarly, triazine derivatives presented anticorrosive activity in aluminum and steel in acidic me-

dium [34] [35] [36] [37]. In addition, compounds containing the morpholine group exhibited anticorrosive activity, mainly in steel, in acidic media [38] [39].

From this perspective, this work aims to synthesize, characterize, and evaluate the corrosion inhibition efficiency of molecular hybrids containing the 1,4-NQ, quinoline, triazine and morpholine cores, shown below (**Figure 1**). These compounds were synthesized through successive aromatic nucleophilic substitution (S_NAr) reactions in cyanuric chloride using morpholine and the intermediates containing 1,3-propanediamine linked to quinoline and naphthoquinone core as nucleophiles. All synthesized compounds were characterized by infrared, and ^1H and ^{13}C NMR spectroscopy and high-resolution mass spectrometry. Anti-corrosion activity was determined through potentiodynamic polarization and electrochemical impedance studies. More details can be found in the subsequent sections.

2. Experimental Part

All solvents and starting materials were commercially available and used without any previous treatment.

The melting point determinations of starting materials, intermediates, and final products were carried out on the Fisatom 430D digital equipment. Infrared spectra of the synthesized molecules were obtained on the Perkin Elmer Spectrum 400 spectroscope, using as parameters: 16 scans and a resolution length of 4 cm^{-1}, in Attenuated Total Reflectance (ATR) mode, with horizontal zinc selenide (ZnSe) crystal. All analyzes were performed in a wavelength range of 4000 to 650 cm^{-1}. ^1H and ^{13}C NMR spectra were obtained on a Varian 400 MHz spectrometer with 5 mm Broadband 1H/X/D probe. Chemical shifts (δ) are expressed in parts per million (ppm) relative to the internal standard (TMS). Solvents used were $CDCl_3$ (CIL, 99.8%), DMSO-d_6 (Sigma-Aldrich, 99.9%), and MeOD (Aldrich, 99.8%).

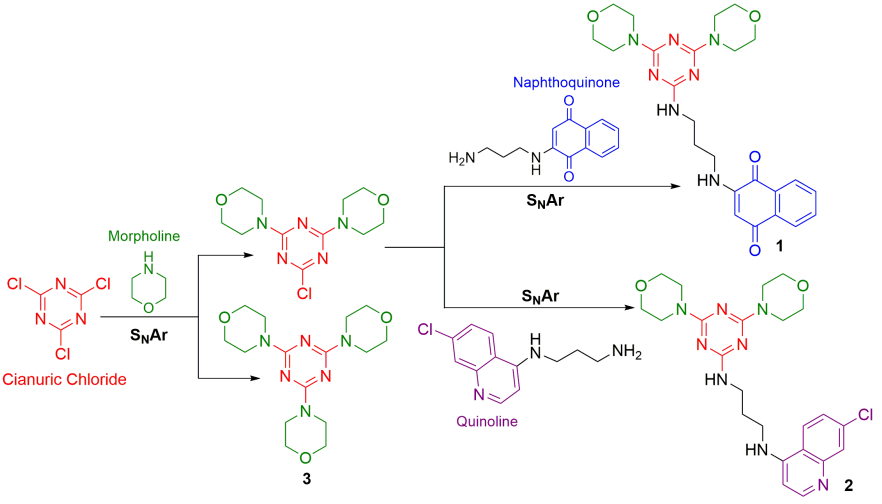

Figure 1. Molecular hybrids containing morpholine, 1,4-naphthoquinone, quinoline and 1,3,5-triazine cores.

Mass spectra were obtained on the high resolution spectrometer (model 9.4 T Solarix, Bruker Daltonics, Bremen, Germany), operated in positive ionization modes with ionizing electrospray, ESI(+)-FT-ICR (MS). The acquisition of FT-ICR MS spectra was performed with a resolution power of m/Δm50% ≈ 500,000, where Δm50% is the integer peak, with m/z 400 being half the maximum height and mass accuracy < 1 ppm.

2.1. Synthesis

Synthesis of 2-Methoxylawsone (**5**)

In a 1000 mL round bottom flask, lawsone **4** (10.000 g, 57.4 mmol) was added to 350 mL of methanol with 11 mL of concentrated hydrochloric acid under magnetic stirring. The reaction mixture was maintained under reflux until total consumption of the lawsone. This procedure was accompanied by thin layer chromatography. Then, the reaction mixture was allowed to reach room temperature and the crude product was filtered and recrystallized from hot ethanol to achieve a pale yellow solid in 77% yield, 8.320 g; mp: 188˚C - 190˚C (lit.: 182˚C - 183˚C); IR (ATR): ν = 3049.5 (w), 2991 (w) (CH_3), 1681 (s) (C=O), 1643 (s) (conjugated C=C), 1603 (vs) (C=C), 1214 (s) (C-O-C), 1044 (s) cm^{-1} (C-O-C); ^1H NMR (400 MHz, $CDCl_3$): δ = 8.12 (m, 2H; Ar-H), 7.76 (m, 2H; Ar-H), 6.19 (s, 1H; CCH), 3.92 ppm (s, 3H; CH_3); ^{13}C NMR (101 MHz, $CDCl_3$): δ = 184.8 (C=O), 180.1 (C=O), 160.4 (C-O), 134.3 (Ar), 133.3 (Ar), 132.0 (Ar), 131.0 (Ar), 126.7 (Ar), 126.2 (Ar), 109.9 (CCH), 56.4 ppm (CH_3).

Synthesis of 2-((3-Aminopropyl)amino)naphthalene-1,4-dione (**6**)

In a 500 mL round bottom flask, 2-methoxylawsone **8** (0.941 g, 5 mmol) was added to 100 mL of absolute methanol, 1,3-diaminopropane (840 µL, 10 mmol) and triethylamine (840 µL, 6 mmol). The reaction mixture was stirred for 24 h at room temperature. After that time, 150 mL of distilled water was slowly added and the methanol was partially evaporated on a rotary evaporator to precipitate the product in the solution, which was then filtered and washed with cold methanol. Purification of the crude product was done by recrystallization with a 30% water/methanol mixture. An orange solid was obtained in 71% yield, 0.818 g; mp 130˚C - 131˚C (lit.: 124˚C - 126˚C); IR (ATR): ν = 3354 (m) (NH), 2960 (w) (CH_2), 1669 (m) (C=O), 1642 (s) (C=O), 1603 (vs) (conjugated C=C), 1242 (m) cm^{-1} (CN); ^1H NMR (400 MHz, $CDCl_3$): δ = 8.09 (m, 1H; Ar-H), 8.03 (m, 1H, Ar-H), 7.71 (td, 1H, J = 7.6, 1.4 Hz; Ar-H), 7.60 (td, 1H, J = 7.5, 5.9, 1.3 Hz; Ar-H), 6.82 (s, 1H; NH), 5.72 (s, 1H; CCH), 3.29 (dd, 2H, J = 12.3, 6.3 Hz; CH_2-NH), 2.90 (t, 2H, J = 6.4 Hz; CH_2-NH_2), 1.83 ppm (m, 2H; CH_2); ^{13}C NMR (101 MHz, $CDCl_3$): δ = 182.9 (C=O), 182.0 (C=O), 148.3 (C-NH), 134.7 (Ar), 133.7 (Ar), 131.9 (Ar), 130.6 (Ar), 126.2 (Ar), 126.1 (Ar), 100.5 (CCH), 41.4 (CH_2-NH), 40.2 (CH_2-NH_2), 30.8 ppm (CH_2).

Synthesis of 4,4'-(6-Chloro-1,3,5-triazine-2,4-diyl)dimorpholine (**9**) and 2,4,6-trimorpholino-1,3,5-triazine (**3**)

In a 100 mL round bottom flask, cyanuric chloride **7** (5 mmol, 0.922 g), ace-

tone (5 mL), crushed ice (25 g), triethylamine (2 mL) and morpholine **8** (10 mmol, 0.861 mL) were added. The reactional content was kept under stirring and, after reaching the room temperature, the reaction was monitored by thin layer chromatography. After two hours to obtain **9** and five hours for **3**, 10 mL of distilled water at room temperature were added and the reaction content was filtered and washed with distilled water. Compound **9** was obtained as a white solid in 55% yield, 0.786 g, after recrystallization from etanol; mp 177˚C - 179˚C (lit.: 175˚C - 176˚C); IR (ATR): ν = 2851.5 (w) (CH_2), 1541 (vs) (C=N), 1248 (s) (C-N), 1109 (vs) (C-O-C), 856 (s) cm^{-1} (C-Cl); ^1H NMR (400 MHz, $CDCl_3$): δ = 3.75 (m, 2H; CH_2N), 3.69 ppm (m, 2H; CH_2O); ^{13}C NMR (101 MHz, $CDCl_3$): δ = 169.6 (aromatic C), 164.4 (C-Cl), 66.8 (C-O), 43.8 ppm (C-N); HRMS (FT-ICR MS-ESI+) m/z calcd. for $[C_{11}H_{16}ClN_5O_2 + H]^+$: 286.10653, found: 286.10682 (err = −1.02 ppm). Compound **3**, in turn, was obtained in 32% yield, 0.538 g, also as a white solid, after recrystallization from ethanol. Decomp.: 275˚C - 277˚C (lit.: 284˚C - 289˚C); IR (ATR): ν = 2852 (w) (CH_2), 1539 (vs) (C=N), 1249 (vs) (C-N), 1107 (vs) (C-O-C) cm^{-1}; ^1H NMR (400 MHz, $CDCl_3$): δ = 3.73 (m, 2H; CH_2N), 3.69 ppm (m, 2H; CH_2O); ^{13}C NMR (101 MHz, $CDCl_3$): δ = 165.1 (aromatic C), 66.8 (C-O), 43.7 ppm (C-N); HRMS (FT-ICR MS-ESI+) m/z calcd. for $[C_{14}H_{24}N_6O_3 + H]^+$: 337.19827, found: 337.19812 (err = 0.42 ppm).

Synthesis of 2-((3-((4,6-Dimorpholino-1,3,5-triazin-2yl)amino)propyl)amino) naphthalene-1,4-dione **(1)**

The aminonaphthoquinone **6** (0.5 mmol, 0.115 g) was solubilized in 20 mL of acetonitrile under magnetic stirring and reflux in a 50 mL round bottom flask. Then, 4,4'-(6-chloro-1,3,5-triazine-2,4-diyl)dimorpholine **9** (0.5 mmol, 0.143 g) and triethylamine (70 µL) were added. The reaction was monitored by thin layer chromatography and, after 16 h, the reaction content was filtered, although the limiting starting material was not completely consumed, to prevent the formation of byproducts. The pure product was obtained as a yellow solid, after recrystallization from hot ethanol, in 34% yield, 0.0814 g; mp: 211˚C - 213˚C (lit.: 210°C - 212°C); IR (ATR): ν = 3377 (m) (NH), 2952 (w) (CH_2), 2853 (w) (CH_2), 1681 (m) (C=O), 1605 (s) (conjugated C=C), 1548 (vs) (C=N), 1251 (vs) (C-N), 1105 (vs) cm^{-1} (C-O-C); ^1H NMR (400 MHz, DMSO-d_6): δ = 7.95 (d, 1H, J = 7.6 Hz; Ar-H), 7.90 (d, 1H, J = 7.6 Hz; Ar-H), 7.79 (t, 1H, J = 7.5 Hz; Ar-H), 7.69 (t, 1H, J = 7.5 Hz; Ar-H), 7.52 (t, 1H, J = 6.1 Hz; NH), 6.83 (t, 1H, J = 5.9 Hz; NH), 5.63 (s, 1H; CCH), 3.42 (m, 16H; morpholines CH_2-O and CH_2-N), 3.21 (m, 4H; CH_2-NH), 1.75 ppm (m, 1H; CH_2); ^{13}C NMR (101 MHz, DMSO-d_6): δ = 182.0 (C=O), 181.6 (C=O), 166.2 (triazine C linked to morpholines), 165.1 (triazine C linked to diamine), 148.9 (naphthoquinone C linked to diamine), 135.3 (Ar), 133.6 (Ar), 132.6 (Ar), 130.8 (Ar), 126.3 (Ar), 125.8 (Ar), 99.7 (C=CNH), 66.5 (morpholine C-O), 43.6 (morpholine C-N), 38.1 (diamine C-NH), 27.9 ppm (diamine CH_2); HRMS (FT-ICR MS-ESI+) m/z calcd. for $[C_{24}H_{29}N_7O_4 + H]^+$: 480.23538, found: 480.23549 (err = −0.23 ppm), calcd. for dimer $[C_{48}H_{58}N_{14}O_8$ +

H]$^+$: 959.46348, found: 959.46450 (err = −1.06 ppm).

Synthesis of N^1-(7-Chloroquinolin-4-yl)propane-1,3-diamine (**11**)

In a 25 mL round bottom flask, 2.0 g (10.1 mmol) of 4,7-dichloroquinoline **10** and 4.2 mL of 1,3-diaminopropane were mixed. The mixture was heated to 80˚C, without stirring, until the complete solubilization of 4,7-dichloroquinoline. The solution was then stirred for 1 h at 120˚C until the consumption of 4,7-dichloroquinoline, verified by thin-layer chromatography. Then, the reaction content was transferred to a beaker containing crushed ice, to which 20 mL of cold water was added. The precipitate formed was filtered and washed with cold water. The solid obtained was stirred with ethyl acetate (15 mL) and further filtered to achieve a white solid in 74% yield, 1.761 g. However, it was not possible to purify it because of its low solubility in the organic solvents tested; IR (ATR): ν = 3258 (w) (NH), 2936 (w) (CH_2), 2865 (w) (CH_2), 1540 (vs) (C=N), 852 (m) cm^{-1} (C-Cl); ^{1}H NMR (400 MHz, DMSO-d_6 1:1 MeOD): δ = 8.40 (d, 1H, J = 5.4 Hz; CH = N), 8.18 (d, 1H, J = 9.0 Hz; Ar-H), 7.80 (d, 1H, J = 2.2 Hz; Ar-H), 7.46 (dd, 1H, J = 9.0, 2.2 Hz; Ar-H), 6.59 (d, 1H, J = 5.4 Hz; Ar-H), 3.44 (t, 2H, J = 7.0 Hz; CH_2-NH), 2.81 (t, 2H, J = 7.0 Hz; CH_2-NH_2), 1.95-1.86 ppm (m, 2H; CH_2); ^{13}C NMR (101 MHz, DMSO-d_6): δ = 152.4 (Ar), 150.5 (Ar), 149.5 (Ar), 133.8 (Ar), 127.9 (Ar), 124.5 (Ar), 124.4 (Ar), 117.9 (Ar), 99.0 (Ar), 40.6 (diamine C-NH), 39.3 (diamine C-NH_2), 30.9 ppm (diamine central C).

Synthesis of N^1-(7-Chloroquinolin-4-yl)-N^3-(4,6-dimorpholino-1,3,5-triazin-2-yl) propane-1,3-diamine (**2**)

Aminoquinoline **11** (0.5 mmol, 0.118 g) was solubilized in 20 mL of acetonitrile, under stirring and refluxing, in a 50 mL round bottom flask. Then 4,4'-(6-chloro-1,3,5-triazine-2,4-diyl)dimorpholine **9** (0.5 mmol, 0.143 g) and triethylamine (70 μL) were added. The reaction was monitored by thin layer chromatography and, after 16 h, the reaction content was filtered, although the limiting starting material was not completely consumed, to avoid the formation of byproducts. The pure product was obtained as a white solid, after recrystallization from hot methanol, in 35% yield, 0.0850 g; mp 225˚C - 227˚C (lit.: 230˚C - 231˚C); IR (ATR): ν = 3360 (w) (NH), 2965 (w) (CH_2), 2862 (w) (CH_2), 1546 (vs) (C=N), 1259 (s) (C-N), 1108 (s) (C-O-C), 852 (m) cm^{-1} (C-Cl); ^{1}H NMR (400 MHz, DMSO-d_6): δ = 8.34 (d, 1H, J = 5.3 Hz, 1H; CH = N), 8.21 (d, 1H, J = 9.0 Hz; Ar-H), 7.74 (d, 1H, J = 1.4 Hz; Ar-H), 7.41 (dd, 1H, J = 9.0, 1.4 Hz; Ar-H), 7.29 (t, 1H, J = 5.3 Hz; NH), 6.86 (t, 1H, J = 5.8 Hz, 1H; NH), 6.41 (d, 1H, J = 5.3 Hz; Ar-H), 3.45 (m, 16H; morpholines CH_2-O and CH_2-N), 3.27 (m, 4H; CH_2-NH), 1.83 ppm (m, 2H; CH_2); ^{13}C NMR (101 MHz, DMSO-d_6): δ = 166.1 (triazine C linked to morpholines), 165.1 (triazine C linked to morpholines), 152.3 (Ar), 150.4 (Ar), 149.5 (Ar), 133.8 (Ar), 127.9 (Ar), 124.4 (Ar), 117.9 (Ar), 99.1 (Ar), 66.5 (morpholine C-O), 43.5 (morpholine C-N), 38.4 (diamine C-NH), 28.3 ppm (diamine CH_2); HRMS (FT-ICR MS-ESI+) m/z calcd. for [$C_{23}H_{29}ClN_8O_2$ + H]$^+$: 485.21748, found: 485.21776 (err = −0.58 ppm).

2.2. Evaluation of the Corrosion Activity

The evaluation of the anticorrosive activity was performed by electrochemical tests using a 100 mL capacity eletrochemical cell of three electrodes: reference Hg/HgO (Analion), carbon counter (4.00 cm^2), and AISI 316 stainless steel as working electrode, with areas of 16.234 cm^2, 17.768 cm^2 and 18.286 cm^2. The stainless-steel surface were treated with 120, 400, and 600 sands. Analyses were carried out in 50 mL simulated water production solutions containing 150,000 $mg{\cdot}L^{-1}$ of chloride ions (Cl^-) and 5 $mg{\cdot}L^{-1}$ of sulphide ions (S^{2-}), that were prepared with NaCl (Dinâmica) and Na_2S (Impex). The compounds tested were weighed and dissolved in a small amount of DMSO (dimethylsulfoxide) (**Table 1**) and then added to the electrolytic solution containing Cl^- and S^{2-}, presenting the final concentrations of 20, 30, 50 and 100 $mg{\cdot}L^{-1}$. Blanks were prepared with the volumes of DMSO used to solubilize the compounds at the tested concentrations and the solution containing Cl^- and S^{2-}.

Potentiodynamic Polarization and impedance measurements were performed without stirring at room temperature in the AUTOLAB 302 potentiostat/galvanostat. The Potentiodynamic Polarization measurements were performed with a scan rate of 1 $mV{\cdot}s^{-1}$ in a potential range of ±100 mV around the open circuit potential, which was determined before the polarization and EIS (Electrochemical Impedance Spectroscopy) studies for a period of 3600s. The corrosion inhibition efficiencies for the different inhibitor concentrations were calculated using the following equation (Equation (1)) [40]:

$$\eta p(\%) = \frac{i_0 - i_1}{i_0} \times 100 \tag{1}$$

where i_0 and i_1 are the corrosion current densities, obtained from the extrapolation of potentiodynamic polarization curves in the absence and presence of the inhibitor, respectively. EIS is one of the most important techniques for studying the strength characteristics of the film formed on the metal surface, which provides information on the corrosive process [41]. EIS measurements were made in a frequency range from 0.1 mHz to 100 kHz, with amplitude of 10 mV p/p. The potential applied was −0.25 V. The simulation of impedance data obtained was performed in the EIS Spectrum Analyzer Software [42], using the electrical equivalent circuit shown in **Figure 2**, where R1 is associated with the solution resistance, R2 is the resistance of the inhibitor film coating the surface of AISI 316 stainless steel, CPE-1 is the constant phase element associated with the inhibitor film, R3 is the charge transfer resistance of the interface and, finally, CPE-2 is the constant phase element associated with the double electric layer. Data were adjusted with errors below 10% and chi-square at 10^{-3}.

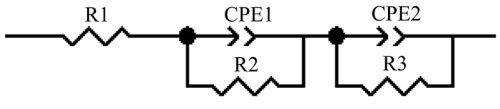

Figure 2. Electrical equivalent circuit used to adjust the data obtained in the impedance test.

Table 1. DMSO volumes used to solubilize the compounds synthesized at each concentration tested and for the preparation of the blanks.

Compound	Concentration/(mg·L^{-1})	DMSO Volume/mL
1	20	1
	30	2
	50	4
	100	5
2	20	1
	30	1
	50	2
	100	2
3	20	2
	30	2
	50	4
	100	5

2.3. Computational Investigation

Full geometry optimizations were carried out using the B3LYP[18] functional together with the 6-31+g(d,p) basis set. For each optimized stationary point, the second-order Hessian matrix was computed at the same level to confirm the stationary point as a minimum on the potential energy surface, in which all Hessian eigenvalues are positive. The normal mode calculations were also useful for computing the thermodynamic parameters at 298 K using standard statistical thermodynamic equations for an ideal gas [43]. Next, the optimized geometries were used for single point calculations using the M06-2X [44] and PBE0 [45] functionals together with the 6-311+g(d,p) basis set. For both geometry optimization and single point calculations solvation effects were also accounted for by using dimethyl sulfoxide (DMSO) as solvent with the IEFPCM polarized continuum solvation model [46] [47]. All computations were performed with the G09 software package using default convergence criteria [48].

3. Results and Discussion

Our first goal was to prepare the molecular hybrids **1** and **2** and the triazine derivative **3**. The hybrids are formed from molecular blocks (containing the naphthoquinone and triazine cores for **1** and quinoline and triazine cores for **2**) which itself had to be prepared, as described below. To prepare the nucleophilic precursor of the hybrid compound **1**, we started from lawsone **4**, used to synthesize the 2-methoxylawsone **5** as a yellow solid in 77% yield, following a methodology described in the literature [49]. Reacting 2-methoxylawsone **5** with 1,3-diaminopropane, in methanol in the presence of triethylamine for 24 h, yielded the aminonaphthoquinone **6** as an orange solid in 71% yield, following a procedure described by our research group [50] (**Figure 3**). The reaction me-

chanism to form **6** from 1,3-diaminopropane and 2-methoxylawsone should be similar to that recently proposed by our group [51], in which the reaction occurs in a single asynchronous step, involving an addition-elimination process in a decoupled S_N2 mechanism, *i.e.*, with one step and two stages, in which the second stage (rupture of the carbon - leaving group bond) occurs with low or no activation energy.

The electrophilic precursor to the molecular hybrid **1** (compound **9**) and the triazine derivative **3** were obtained by nucleophilic aromatic substitution reactions (S_NAr) between cyanuric chloride **7** and morpholine **8**, in presence of triethylamine and acetone with crushed ice as solvent (**Figure 4**) [52]. The morpholine group was chosen intending to increase the solubility of intermediate **9** in usual organic solvents, facilitating the homogeneity of subsequent reactions [23] [24]. After two hours of reaction at room temperature, product **9** was obtained as a white solid in 55% yield. Extending the reaction time to five hours, compound **3** was obtained in 32% yield, also as a white solid. The mass spectra of compounds **3** and **9** allowed distinguishing their chemical composition. The mass spectrum of compound **3** shows a single peak with mass/charge ratio of 337.19812 m/z (error 0.42 ppm), relative to the protonated compound. In the mass spectrum of **9**, a peak with mass/charge ratio of 286.10682 m/z (error −1.02 ppm) relative to the protonated compound was identified, as well as the typical isotopic standard of the chlorine atom. The melting point of compound **9** is in the range of 177˚C - 179˚C (lit.: 175˚C - 176˚C), while compound **3** decomposes in the temperature range of 275˚C - 277˚C (lit.: 284˚C - 289˚C).

Having both, the nucleophilic derivative **6** and the electrophilic intermediate **9**, the molecular hybrid **1** was obtained as a yellow solid in 34% yield by reacting **6** with **9** in acetonitrile for 16 hours, under reflux in the presence of triethylamine (**Figure 5**) [23]. Two important peaks were observed in the mass spectrum of **1**: one in the mass/charge ratio of 480.23549 m/z (error of −0.23 ppm), related to the protonated species; and one in the mass/charge ratio of 959.46450 m/z (error of −1.06 ppm), associated to the protonated dimer.

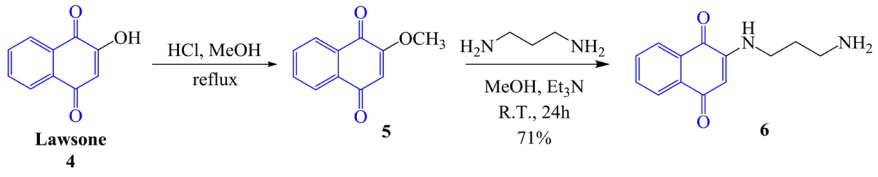

Figure 3. Synthesis of compound **6**.

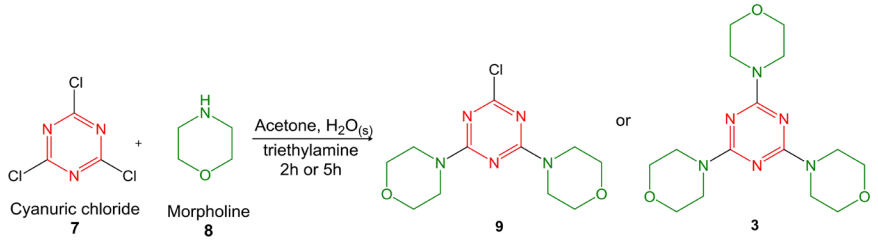

Figure 4. Synthesis of compounds **3** and **9**.

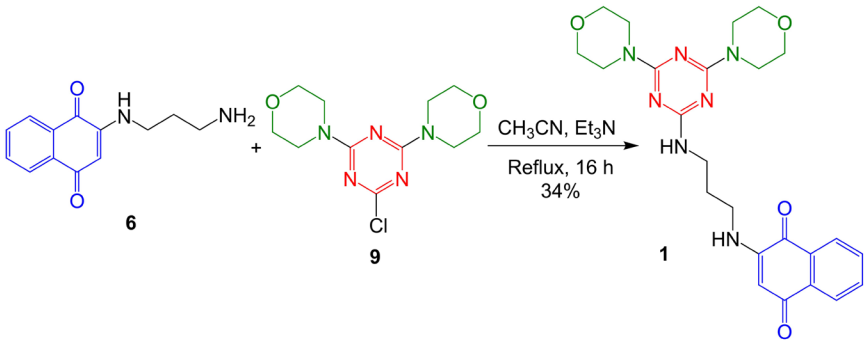

Figure 5. Synthesis of the target molecular hybrid 1.

To prepare the molecular hybrid **2**, we used the same intermediate **9** obtained before and reacted it with aminoquinoline **11**, which was obtained by an S_NAr reaction between 4,7-dichloroquinoline **10** and 1,3-diaminopropane (**Figure 6**), following the experimental conditions described by Carmo *et al.* [53].

The reaction was carried out in excess of 1,3-diaminopropane at 80˚C - 110˚C for one hour. The aminoquinoline **11** was obtained as a white solid in 74% yield. When reacting **9** and **11**, the molecular hybrid **2** was obtained after 16 hours as a white solid in 35% yield. In the mass spectrum of **2**, we identified a peak related to the protonated compound, with a mass/charge ratio of 485.21776 m/z (error of −0.58 ppm).

After synthesizing the three target compounds (**1**, **2** and **3**) we evaluated their efficiency for protecting AISI 316 stainless steel against corrosion. Potentiodynamic polarization curves were obtained in the absence and in the presence of compounds **1**, **2** and **3** at different concentrations (**Figures 7-9**). These figures also show the results obtained with a blank solution for each concentration.

For compound **1** at low concentration (20 $mg{\cdot}L^{-1}$) the corrosion potential is below −0.15 V vs. Hg/HgO (**Figure 7**). The cathodic current density decreases regarding the blank, while the anodic current density increases.

At concentration of 30 $mg{\cdot}L^{-1}$, both current densities are higher, showing low inhibitory efficiency at these concentrations. At concentrations above 50 $mg{\cdot}L^{-1}$, it was possible to observe the beginning of the corrosion inhibition process because the corrosion potential was slightly higher for **1** than for the blank (*i.e.*, E_{corr} = −0.205 V vs. Hg/HgO for **1** and E_{corr} = −0.209 V vs. Hg/HgO for the blank). At a concentration of 100 $mg{\cdot}L^{-1}$, the inhibition effect is quite pronounced (E_{corr} = −0.123 V vs. Hg/HgO for **1** and E_{corr} = −0.136 V vs. Hg/HgO for the blank). Moreover, both anodic and cathodic current densities in the presence of compound **1** present values much smaller than for the blank. Thus, at the concentration of 100 $mg{\cdot}L^{-1}$ compound **1** shows high efficiency in inhibiting the corrosion process in AISI 316 stainless steel (*i.e.*, $\eta\rho$ = 85.67%).

Figure 8 shows the behavior when testing compound **2**. In contrast to compound **1**, in all investigated concentrations (20 $mg{\cdot}L^{-1}$, 30 $mg{\cdot}L^{-1}$, 50 $mg{\cdot}L^{-1}$ and 100 $mg{\cdot}L^{-1}$) compound **2** shows an increased corrosion potential when com-

pared to the blank. All curves show the same profile, that is, a decrease in the anodic current density and an increase in the cathodic current density, except for the 50 mg·L^{-1} concentration, where the cathodic current density shows the same profile as the blank. Such behavior is an evidence for the inhibitory power of compound **2** under the experimental conditions investigated (E_{corr} = −0.126 V vs. Hg/HgO for **2** and E_{corr} = −0.174 V vs. Hg/HgO for the blank; $\eta\rho$ = 76.26%).

Finally, Figure 9 shows the behavior observed for compound **3**. The same profile obtained with compound **2** was also observed here, showing that both compounds **2** and **3** present the same corrosion inhibiting behavior for AISI 316 stainless steel under the conditions investigated, although at concentration of 100 mg·L^{-1}, compound **3** present the same cathodic current density profile as the blank.

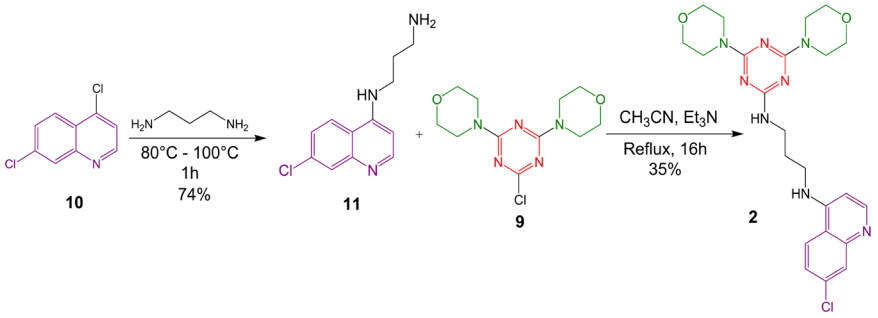

Figure 6. Synthesis of the molecular hybrid **2**.

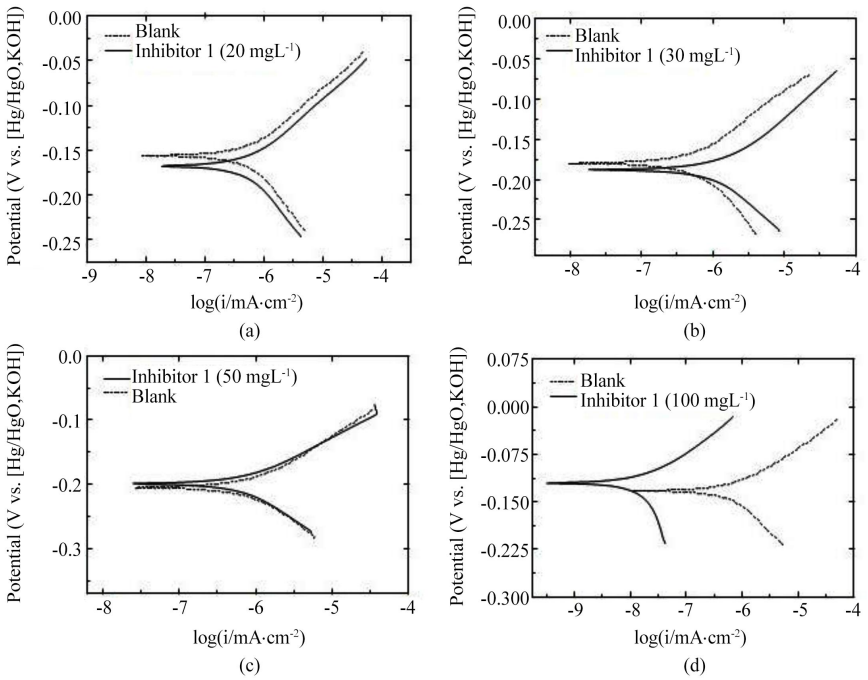

Figure 7. Potentiodynamic polarization curves of AISI 316 stainless steel for the blank and in the presence of compound **1** at different concentrations.

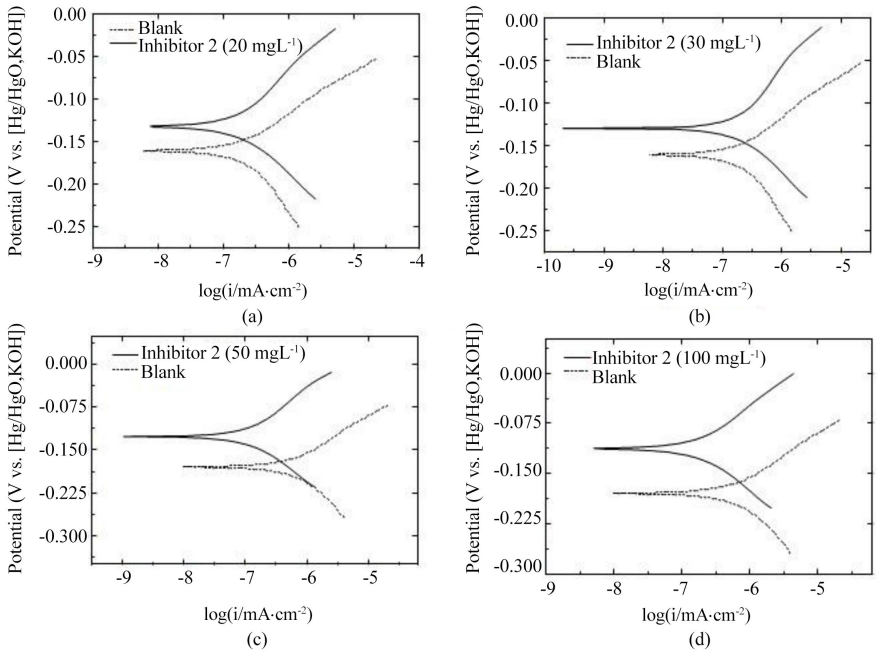

Figure 8. Potentiodynamic polarization curves of AISI 316 stainless steel for the blank and in the presence of compound 2 at different concentrations.

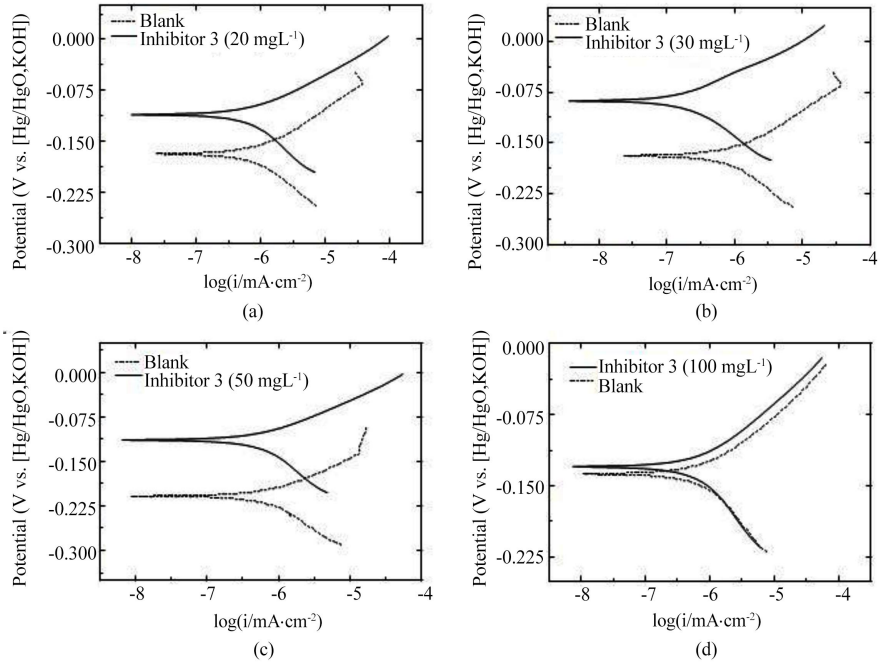

Figure 9. Potentiodynamic polarization curves of AISI 316 stainless steel for the blank and in the presence of compound **3** at different concentrations.

Based on the Pourbaix [54] diagram and the potentiodynamic polarization curves obtained, it was possible to observe that the AISI 316 stainless steel sample undergo mild pitting corrosion or uniform corrosion.

All the compounds investigated show inhibitory activity in AISI 316 stainless steel for the corrosion process in the presence of chloride or sulphide ions, at all

concentrations used, exception made for concentrations of 20 and 30 mg·L^{-1} for compound **1**. Regarding inhibition efficiency, compound **1** shows the best value (85.67%) at the concentration of 100 mg·L^{-1}, followed by compound **2** with 76.26% efficiency at concentration of 50 mg·L^{-1} and, finally, 66.65% inhibition efficiency for compound **3** at the concentration of 30 mg·L^{-1}. At the concentrations where the best corrosion inhibition efficiency was achieved, a reduction of the corrosion current density was observed, indicating a lower flow of electrons from the anodic region to the cathodic region. In addition, for a given concentration, the presence of compounds **1**, **2** and **3** shifts the values of the corrosion potentials to more positive values, indicating a strong influence of these compounds on the anodic reaction (iron oxidation).

According to the present data, compound **1** shows characteristic of miscellaneous inhibition. It can act either as anodic or as cathodic inhibitor, due to the displacement of Tafel coefficients βa and βc. In the case of compounds **2** and **3**, the main profile indicates them as anodic inhibitors. This is confirmed by a large variation in the Tafel coefficient βa.

Tables 2-4 present the values for corrosion potentials (E_{corr}) and corrosion current densities (i_{corr}), obtained by the Tafel curve extrapolation method, and the inhibition efficiency values ($\eta\rho$), calculated according to Goulart *et al.* [40].

Table 2. Electrochemical parameters calculated for AISI 316 stainless steel from potentiodynamic polarization measurements in the absence and presence of different concentrations of compound 1 in simulated water production medium containing 150,000 mg·L^{-1} of Cl^- and 5 mg·L^{-1} of S^{2-}.

Compound **1**									
Concentration/ (mg·L^{-1})	E_{corr}/ (V *vs.* Hg/HgO)	E_{corr} blank/ (V *vs.* Hg/HgO)	i_{corr}/ (mA·cm^{-2})	i_{corr} blank/ (mA·cm^{-2})	βa	βc	βa blank	βc blank	η_P/%
20	−0.167	−0.154	4.70×10^{-7}	4.00×10^{-7}	0.05792	−0.08453	0.05901	−0.08968	0.00
30	−0.190	−0.174	8.15×10^{-7}	6.02×10^{-7}	0.07431	−0.09248	0.06489	−0.07755	0.00
50	−0.205	−0.209	5.91×10^{-7}	6.54×10^{-7}	0.06175	−0.06819	0.05562	−0.08614	9.68
100	−0.123	−0.136	1.04×10^{-7}	7.24×10^{-7}	0.06483	−0.29616	0.06018	−0.08681	85.67

Table 3. Electrochemical parameters calculated for AISI 316 stainless steel from potentiodynamic polarization measurements in the absence and presence of different concentrations of compound 2 in simulated water production medium containing 150,000 mg·L^{-1} of Cl^- and 5 mg·L^{-1} of S^{2-}.

Compound **2**									
Concentration/ (mg·L^{-1})	E_{corr}/ (V *vs.* Hg/HgO)	E_{corr} blank/ (V *vs.* Hg/HgO)	i_{corr}/ (mA·cm^{-2})	i_{corr} blank/ (mA·cm^{-2})	βa	βc	βa blank	βc blank	η_P/%
20	−0.131	−0.154	1.56×10^{-7}	4.00×10^{-7}	0.07496	−0.07673	0.05901	−0.08968	61.07
30	−0.127	−0.154	1.60×10^{-7}	4.00×10^{-7}	0.10503	−0.08078	0.05901	−0.08968	60.08
50	−0.126	−0.174	1.43×10^{-7}	6.02×10^{-7}	0.09082	−0.08482	0.06489	−0.07755	76.26
100	−0.115	−0.174	1.64×10^{-7}	6.02×10^{-7}	0.07993	−0.08715	0.06489	−0.07755	72.78

Table 4. Electrochemical parameters calculated for AISI 316 stainless steel from potentiodynamic polarization measurements in the absence and presence of different concentrations of compound 3 in simulated water production medium containing 150,000 mg·L^{-1} of Cl^- and 5 mg·L^{-1} of S^{2-}.

Compound **3**									
Concentration/ (mg·L^{-1})	E_{corr}/ (V *vs.* Hg/HgO)	E_{corr} blank/ (V *vs.* Hg/HgO)	i_{corr}/ (mA·cm^{-2})	i_{corr} blank/ (mA·cm^{-2})	βa	βc	βa blank	βc blank	η_P/%
20	−0.119	−0.174	5.12×10^{-7}	6.02×10^{-7}	0.06278	−0.08243	0.06489	−0.07755	14.89
30	−0.0856	−0.174	2.01×10^{-7}	6.02×10^{-7}	0.04977	−0.07702	0.06489	−0.07755	66.65
50	−0.123	−0.209	5.82×10^{-7}	6.54×10^{-7}	0.04806	−0.09786	0.05562	−0.08614	11.01
100	−0.134	−0.136	6.47×10^{-7}	7.24×10^{-7}	0.05454	−0.08851	0.06018	−0.08681	10.61

To better understand the inhibition process of the synthesized compounds, they were systematically studied by Electrochemical Impedance Spectroscopy (EIS). **Figure 10(a)**, **Figure 10(c)** and **Figure 10(e)** show the complex plane impedance plots for the AISI 316 stainless steel, obtained in the presence of different concentrations of the three compounds, in the electrochemical potential of −0.25 V vs. Hg/HgO (this electrochemical potential was chosen due to the best signal/noise ratio). According to **Figures 10(a)-(e)**, all impedance spectra are deformed semicircles and the profiles present relatively low imaginary (-Zimag) and real (Zreal) impedance values as a function of concentration, except for compound **1** at 100 mg·L^{-1} (**Figure 10(a)**), which presented a high Zreal value of 253,050 Ω cm^2. This is consistent with the potentiodynamic polarization results, which evidenced the higher corrosion inhibition efficiency (*i.e.* 85.67%) at this concentration. In addition, when comparing the impedance spectra of the other compounds, the highest values of real and imaginary impedances are observed for the same concentrations of higher inhibition efficiency obtained in the potentiodynamic polarization studies, that is, the higher resistance is associated with higher efficiency against the corrosion process.

Figure 10(b), **Figure 10(d)** and **Figure 10(f)** show the Bode plots for AISI 316 stainless steel obtained in the presence of different concentrations of the three compounds, in the electrochemical potential of −0.25 V vs. Hg/HgO. Two contrasting behaviours can be observed: first, compound **1** presents lower $-\theta$ (phase angle) than compounds **2** and **3**, being ~30˚ for the concentration of 100 mg·L^{-1} and ~60˚ for the other concentrations. For compounds **2** and **3**, that phase angle ranges from 60˚ - 75˚; second, compound **1** shows a much higher broadening of phase angle with frequency range than compounds **2** and **3**, ranging from **1** to 1000 Hz for concentrations of 20 - 50 mg·L^{-1}. At the concentration of 100 mg·L^{-1}, such range is even broader. The broadening of phase angle with frequency is evidence for the presence of several time constants associated with the inhibition/corrosion process. Such behaviour is typical of electrochemical systems [55] [56].

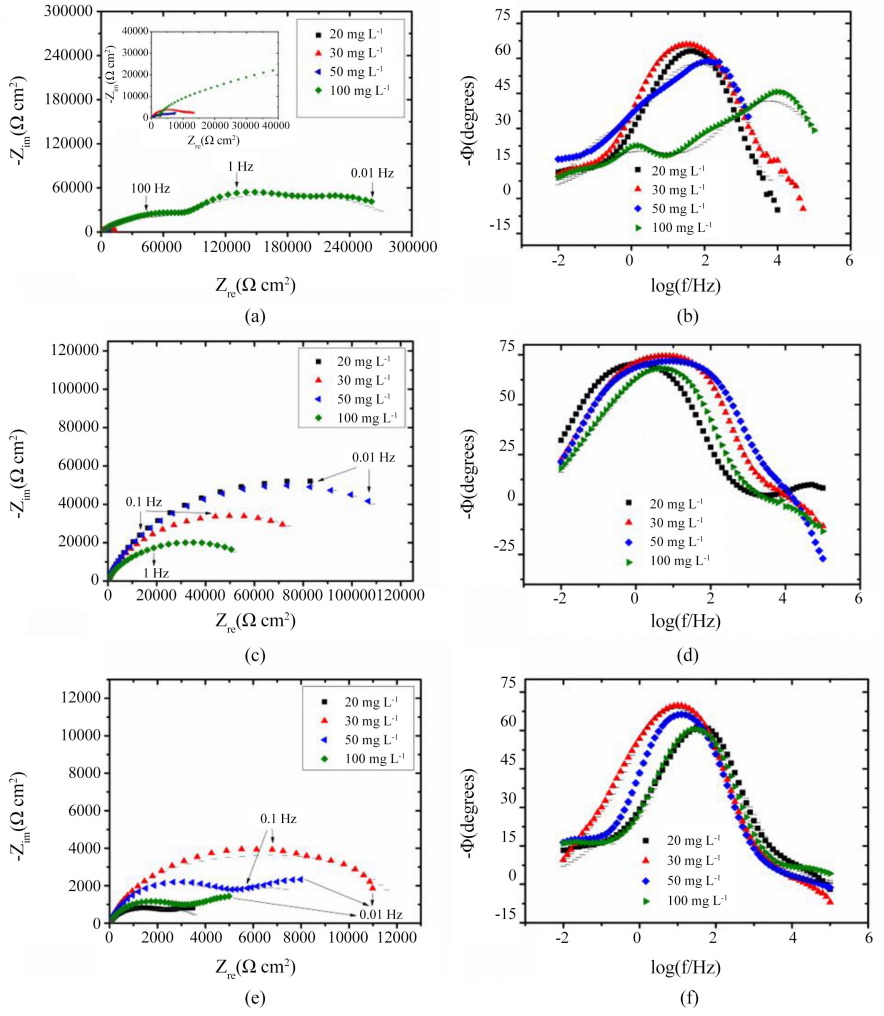

Figure 10. Complex plane impedance and Bode plots of the AISI 316 stainless steel obtained in the presence of different concentrations (20 mg·L^{-1}, 30 mg·L^{-1}, 50 mg·L^{-1} and 100 mg·L^{-1}) of the three corrosion inhibitors, at the electrochemical potential of −0.25 V vs. Hg/HgO, in simulated water production medium containing 150,000 mg·L^{-1} of Cl^- and 5 mg·L^{-1} of S^{2-}. Inhibitor **1** ((a) Complex plane impedance plot, (b) Bode plot); Inhibitor **2** ((c) Complex plane impedance plot, (d) Bode plot); Inhibitor **3** ((e) Complex plane impedance plot, (f) Bode plot).

The best electrical equivalent circuit describing the system was as follows: R1(R2CPE-1) (R3CPE-2), where R1 is associated with the solution resistance, R2 is the resistance of the inhibitor film coating the surface of AISI 316 stainless steel, CPE-1 is the constant phase element associated with the inhibitor film, R3 is the charge transfer resistance of the interface and, finally, CPE-2 is the constant phase element associated with the capacitive characteristics of the system (**Figure 2**—Experimental Part). The impedance of the constant phase element is given by the following mathematical expression: ZCPE = $Q(jw)^{-n}$ [57]. For a pure capacitor $n = 1.0$ and for a pure resistor $n = 0$.

Molecules **1**, **2** and **3** were further investigated regarding their molecular properties, such as HOMO and LUMO energies, hardness, and dipole moment

(Table 5), to associate these molecular properties to the anticorrosive efficiency. The chemical hardness of the molecules was calculated according to Equation (2). The DFT results showed similar trends for both functional used here (M06-2X and PBE0) and for this reason only the values obtained using the M06-2X functional will be discussed in detail. All molecules were submitted to conformation search beforehand. However, for molecules **1** and **2** only conformers presenting a linear configuration of the diamine alkyl side chain were considered, as this is most likely to be the structural configuration after adsorption on the steel surface.

$$\eta = \frac{E_{\text{HOMO}} - E_{\text{LUMO}}}{2} \tag{2}$$

All three compounds presented similar HOMO energies, ranging from −7.582 to −7.784 eV when the M06-2X functional was used. On the other hand, the LUMO energies, as well as the chemical hardness varied significantly for the three molecules, with calculated E_{LUMO} values being −2.413, −1.096 and 0.135 eV and hardness values of −2.655, −3.243 and −3.960 eV for compounds **1**, **2** and **3**, respectively. It is worth noticing that compound **1**, which presented the best corrosion inhibition results, had the lowest chemical hardness. In this context, harder compounds are less polarizable, and it could be expected that softer compounds interact more strongly with the metal surface. This may be an indication of the higher efficiency found for compound **1**, when compared to either **2** or **3**. Compounds **2** and **3**, which presented lower inhibition activity than **1**, are those with higher energy LUMOs and higher hardness.

From the charge analysis of these molecules (Figure 11), we observed that the diamine alkyl substituent in **1** and **2** slightly increases the charges over the triazine core when compared to **3**, whereas the presence of either 1,4-naphthoquinone or 7-chloroquinoline in **1** and **2**, respectively, only affects the charge distribution between these same groups and the diamine alkyl chain. This effect could also contribute to the higher inhibition of corrosion presented by these compounds. Compound **1** presents a small positive charge over the diamine alkyl chain and a slightly negative charge over the naphthoquinone moiety, which results in a dipole moment of 4.836 D. For **2** the calculated dipole moment is considerably larger (5.713 D) than that calculated for **1**, as in this case the 7-chloroquinoline and the diamine akyl moieties present larger charge separation.

Table 5. Calculated HOMO and LUMO energies (E_{HOMO} and E_{LUMO}, eV), hardness (η, eV) and dipole moment (Debye) of molecules **1**, **2**, and **3**.

	1		**2**		**3**	
	M06-2X*	PBE0*	M06-2X*	PBE0*	M06-2X*	PBE0*
E_{HOMO}/eV	−7.723	−6.561	−7.582	−6.507	−7.784	−6.561
E_{LUMO}/eV	−2.413	−3.172	−1.096	−1.780	0.135	−0.156
Hardness/η	−5.068	−4.867	−4.339	−4.144	−3.824	−3.359
Dipole/D	4.836	4.820	5.713	5.789	0.210	0.201

*6-311+G(d,p)/IEFPCM(DMSO)//B3LYP/6-31+G(d,p)/IEFPCM(DMSO)

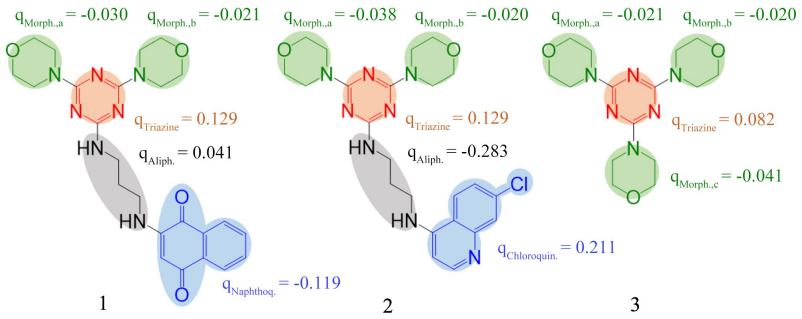

Figure 11. Total ESP charges over 1,3,5-triazine (qTriazine), morpholine (qMorph.), 1,4-naphthoquinone (qNaphthoq.), 7-chloroquinoline (qChloroquin.) moieties, and the aliphatic chain (qAliph.) in the compounds **1-3**.

4. Conclusion

Novel molecular hybrids with relevant anticorrosion activity were obtained in yields ranging from 32% to 35%. The potentiodynamic polarization study showed that the compounds investigated present anticorrosive activity, with corrosion inhibition efficiency ranging from 67% to 86%, and pointed to compound **1** as the best corrosion inhibitor. The analysis of data obtained by electrochemical impedance spectra indicates that such compounds form a protective film on the surface of AISI 316 stainless steel. For inhibitor **1**, the ideal concentration was 100 $mg{\cdot}L^{-1}$, whereas for inhibitors **2** and **3** they were 50 $mg{\cdot}L^{-1}$ and 30 $mg{\cdot}L^{-1}$, respectively. However, the best inhibition efficiency was observed for inhibitor **1**, as it presented a higher Zreal value (253,050 Ω cm^2) when compared with either **2** or **3**. In contrast, the lowest inhibition efficiency of the corrosive process was observed for inhibitor **3**, which presented lower resistance values R2 and R3. In addition, the impedance spectra showed that the higher impedance values were observed for the same concentrations of higher inhibition efficiency obtained in the polarization studies, *i.e.*, a higher resistance is associated with a higher inhibition efficiency for the corrosion process. Molecular properties of the inhibitors were computed by DFT calculations, revealing that lower LUMO energy and smaller chemical hardness of the molecules can be directly correlated to the inhibition efficiency of these molecules.

Acknowledgements

The authors would like to acknowledge the Conselho Nacional de Desenvolvimento Científico e Tecnológico—CNPq, the Coordenadoria de Aperfeiçoamento de Pessoal do Nível Superior—CAPES and the Fundação de Amparo à Pesquisa do Espírito Santo—FAPES for their financial support. JWMC, MD and RGF acknowledge financial support from Fundação de Amparo à Pesquisa do Rio de Janeiro—FAPERJ.

Conflicts of Interest

The authors declare no conflicts of interest regarding the publication of this paper.

References

[1] Pinto, A.V. and De Castro, S.L. (2009) The Trypanocidal Activity of Naphthoquinones: A Review. *Molecules*, **14**, 4570-4590. https://doi.org/10.3390/molecules14114570

[2] Pereyra, C.E., Dantas, R.F., Ferreira, S.B., Gomes, L.P. and Silva-Jr., F.P. (2019) The Diverse Mechanisms and Anticancer Potential of Naphthoquinones. *Cancer Cell International*, **19**, 207.

[3] Hook, I., Mills, C. and Sherida, H. (2014) Bioactive Naphthoquinones from Higher Plants, Studies in Natural Product Chemistry. Elsevier Science Publisher, Amsterdam. https://doi.org/10.1016/B978-0-444-63294-4.00005-X

[4] Shearer, M.J. and Newman, P. (2008) Metabolism and Cell Biology of Vitamin K. *Thrombosis and Haemostasis*, **100**, 530-547. https://doi.org/10.1160/TH08-03-0147

[5] Griffiths, J. (2006) Ullmann's Encyclopedia of Industrial Chemistry. Wiley VCH, Weinheim.

[6] Widhalm, J.R. and Rhodes, D. (2016) Biosynthesis and Molecular Actions of Specialized 1,4-Naphthoquinone Natural Products Produced by Horticultural Plants. *Horticulture Research*, **3**, Article ID: 16046. https://doi.org/10.1038/hortres.2016.46

[7] Ostovari, A., Hoseinieh, S.M., Peikari, M., Shadizadeh, S.R. and Hashemi, S.J. (2009) Corrosion Inhibition of Mild Steel in 1 M HCl Solution by Henna Extract: A Comparative Study of the Inhibition by Henna and Its Constituents (Lawsone, Gallic Acid, α-D-Glucose and Tannic Acid). *Corrosion Science*, **51**, 1935-1949. https://doi.org/10.1016/j.corsci.2009.05.024

[8] Qiu, H.-Y., Wang, P.F., Lin, H.-Y., Tang, C.-Y., Zhu, H.-L. and Yang, Y.-H. (2018) Naphthoquinones: A Continuing Source for Discovery of Therapeutic Antineoplastic Agents. *Chemical Biology & Drug Design*, **91**, 681-690. https://doi.org/10.1111/cbdd.13141

[9] Chaudhary, A., Khurana, J.M. (2016) 2-Hydroxy-1, 4-Naphthoquinone: A Versatile Synthon in Organic Synthesis. *Current Organic Chemistry*, **20**, 1314-1344. https://doi.org/10.2174/1385272820666151125231522

[10] Kumagai, Y., Shinkai, Y., Miura, T. and Cho, A.K. (2011) The Chemical Biology of Naphthoquinones and Its Environmental Implications. Annual Review of Pharmacology, **52**, 221-247. https://doi.org/10.1146/annurev-pharmtox-010611-134517

[11] Marella, A., Tanwar, O.P., Saha, R., Ali, M.R., Srivastava, S., Akhter, M., Shaquiquzzaman, M. and Alam, M.M. (2013) Quinoline: A Versatile Heterocyclic. *Saudi Pharmaceutical Journal*, **21**, 1-12. https://doi.org/10.1016/j.jsps.2012.03.002

[12] Nainwal, L.M., Tasneem, S., Akhtar, W., Verma, G., Khan, M.F., Parvez, S., Shaquiquzzaman, M., Akhter, M. and Alam, M.M. (2019) Green Recipes to Quinoline: A Review. *European Journal of Medicinal Chemistry*, **164**, 121-170. https://doi.org/10.1002/med.21466

[13] Shang, X.-F., Morris-Natschke, S.L., Liu, Y.-Q., Guo, X., Xu, X.-S., Goto, M., Li, J.-C., Yang, G.-Z. and Lee, K.-H. (2018) Biologically Active Quinoline and Quinazoline Alkaloids Part I. *Medicinal Research Review*, **38**, 775-828.

[14] Jain, S., Chandra, V., Jain, P.K., Pathak, K., Pathak, D. and Vaidya, A. (2019) Comprehensive Review on Current Developments of Quinoline-Based Anticancer Agents. *Arabian Journal of Chemistry*, **12**, 4920-4946. https://doi.org/10.1016/j.arabjc.2016.10.009

[15] Chung, P.-Y., Bian, Z.-X., Pun, H.-Y., Chan, D., Chan, A.S.-C., Chui, C.-H., Tang, J.C.-O. and Lam, K.-H. (2015) Recent Advances in Research of Natural and Syn-

thetic Bioactive Quinolines. *Future Medicinal Chemistry*, **7**, 947-967. https://doi.org/10.4155/fmc.15.34

[16] Ram, V.J., Sethi, A., Nath, M. and Pratap, R. (2019) Six-Membered Heterocycles. The Chemistry of Heterocycles. Elsevier, Amsterdam.

[17] Serullas, A. (1828) Annales de Chimie et de Physique, **38**, 379.

[18] Blotny, G. (2006) Recent Applications of 2,4,6-Trichloro-1,3,5-Triazine and Its Derivatives in Organic Synthesis. *Tetrahedron*, **62**, 9507-9522. https://doi.org/10.1016/j.tet.2006.07.039

[19] Sharma, A., El-Faham, A., De La Torre, B.G. and Alberico, F. (2018) Exploring the Orthogonal Chemoselectivity of 2,4,6-Trichloro-1,3,5-Triazine (TCT) as a Trifunctional Linker with Different Nucleophiles: Rules of the Game. *Frontiers in Chemistry*, **6**, 516. https://doi.org/10.3389/fchem.2018.00516

[20] Rapoport, L. and Smolin, E.M. (2009) The Chemistry of Heterocyclic Compounds: s-Triazines and Derivatives. John Wiley & Sons, Hoboken.

[21] Reis, M.I.P., Romeiro, G.A., Damasceno, R.N., Da Silva, F.C. and Ferreira, V.F. (2013) Síntese e Aplicações de 1,3,5-Triazinanas. *Revista Virtual de Química*, **5**, 283-299. https://doi.org/10.5935/1984-6835.20130027

[22] Singla, P., Luxami, V. and Paul, K. (2015) Triazine as a Promising Scaffold for Its Versatile Biological Behavior. *European Journal of Medicinal Chemistry*, **102**, 39-57. https://doi.org/10.1016/j.ejmech.2015.07.037

[23] Fiorot, R.G., Westphal, R., Lemos, B.C., Romagna, R.A., Gonçalves, P.R., Fernandes, M.R.N., Taranto, A.G. and Greco, S.G. (2019) Synthesis, Molecular Modelling and Anticancer Activities of New Molecular Hybrids Containing 1,4-Naphthoquinone, 7-Chloroquinoline, 1,3,5-Triazine and Morpholine Cores as PI3K and AMPK Inhibitors in the Metastatic Melanoma Cells. *Journal of the Brazilian Chemical Society*, **30**, 1860-1873. https://doi.org/10.21577/0103-5053.20190096

[24] Yrjölä, S., Sarparanta, M., Airaksinen, A.J., Hytti, M., Kauppinen, A., Pasonen-Seppänen, S., Adinolfi, B., Nieri, P., Manera, C., Keinänen, O., Poso, A., Nevalainen, T.J. and Parkkari, T. (2015) Synthesis, *in Vitro* and *in Vivo* Evaluation of 1,3,5-Triazines as Cannabinoid CB2 Receptor Agonists. *European Journal of Pharmaceutical Sciences*, **67**, 85-96. https://doi.org/10.1016/j.ejps.2014.11.003

[25] Verma, C., Haque, J., Quraishi, M.A. and Ebenso, E.E. (2019) Aqueous Phase Environmental Friendly Organic Corrosion Inhibitors Derived from One Step Multicomponent Reactions: A Review. *Journal of Molecular Liquids*, **275**, 18-40. https://doi.org/10.1016/j.molliq.2018.11.040

[26] Cardoso, S.P., Reis, F.A., Massapust, F.C., Costa, J.F., Tebaldi, L.S., Araújo, L.F., Silva, M.V.A., Oliveira, T.S., Gomes, J.A.C.P. and Hollauer E. (2005) Avaliação de Indicadores de Uso Diverso como Inibidores de Corrosão. *Química Nova*, **28**, 756-760. https://doi.org/10.1590/S0100-40422005000500004

[27] Vračar, L.M. and Dražićb, D.M. (2002) Adsorption and Corrosion Inhibitive Properties of Some Organic Molecules on Iron Electrode in Sulfuric Acid. *Corrosion Science*, **44**, 1669-1680. https://doi.org/10.1016/S0010-938X(01)00166-4

[28] Nabi, A.S.A. and Hussain, A.A. (2012) Synthesis, Identification and Study of Some New Azo Dyes as Corrosion Inhibitors for Carbon-Steel in Acidic Media. *Journal of Basrah Researches*, **38**, 125-146.

[29] Souza, F.S.D. and Spinelli, A, (2009) Caffeic Acid as a Green Corrosion Inhibitor for Mild Steel. *Corrosion Science*, **51**, 642-649. https://doi.org/10.1016/j.corsci.2008.12.013

[30] Sherif, E.M. and Park, S.M. (2006) Effects of 1,4-Naphthoquinone on Aluminum

Corrosion in 0.50 M Sodium Chloride Solutions. *Electrochimica Acta*, **51**, 1313-1321. https://doi.org/10.1016/j.electacta.2005.06.018

[31] Erdoğan, Ş., Safi, Z.S., Işin, D.Ö., Guo, L. and Kaya, C. (2007) A Computational Study on Corrosion Inhibition Performances of Novel Quinoline Derivatives against the Corrosion of Iron. *Journal of Molecular Structure*, **1134**, 751-761. https://doi.org/10.1016/j.molstruc.2017.01.037

[32] Sundaram, R.G. and Sundaravadivelu, M. (2016) Anticorrosion Activity of 8-Quinoline Sulphonyl Chloride on Mild Steel in 1 M HCl Solution. *Journal of Metallurgy*, **2016**, Article ID: 8095203. https://doi.org/10.1155/2016/8095206

[33] Lgaz, H., Salghi, R., Bhat, K.S., Chaouiki, A. and Shubhalaxmi J.S. (2017) Correlated Experimental and Theoretical Study on Inhibition Behavior of Novel Quinoline Derivatives for the Corrosion of Mild Steel in Hydrochloric Acid Solution. *Journal of Molecular Liquid*, **244**, 154-168. https://doi.org/10.1016/j.molliq.2017.08.121

[34] Karthik, R., Muthukrishnan, P., Elangovan, A., Sri Vidhya, M.M., Jeyaprabha, B. and Prakash, P. (2015) Adsorption and Corrosion Inhibiting Behavior of a New S-Triazine Derivative. *Protection of Metals and Physical Chemistry of Surfaces*, **51**, 667-679. https://doi.org/10.1134/S2070205115040152

[35] El-Fahan, A., Dahlous, K.A., Al Othman, Z.A., Al-Lohedan, H.A. and El-Mahdy, G.A. (2016) Sym-Trisubstituted 1,3,5-Triazine Derivatives as Promising Organic Corrosion Inhibitors for Steel in Acidic Solution. *Molecules*, **21**, 436. https://doi.org/10.3390/molecules21040436

[36] Zhao, Q., Tang, T., Dang, P., Zhang, Z. and Wang, F. (2017) The Corrosion Inhibition Effect of Triazinedithiol Inhibitors for Aluminum Alloy in a 1 M HCl Solution. *Metals*, **7**, 44. https://doi.org/10.3390/met7020044

[37] Obot, I.B., Kaya, S., Kaya, C. and Tüzün, B. (2016) Theoretical Evaluation of Triazine Derivatives as Steel Corrosion Inhibitors: DFT and Monte Carlo Simulation Approaches. *Research on Chemical Intermediate*, **42**, 4963-4983. https://doi.org/10.1007/s11164-015-2339-0

[38] Naji, N.J.N., Ujam, O.T., Ibisi, N.E., Ani, J.U., Onuegbu, T.O., Olasunkanmi, L.O. and Ebenso, E.E. (2017) Morpholine and Piperazine Based Carboxamide Derivatives as Corrosion Inhibitors of Mild Steel in HCl Medium. *Journal of Molecular Liquids*, **230**, 652-661. https://doi.org/10.1016/j.molliq.2017.01.075

[39] Jayanthi, K., Sivaraju, M. and Kannan, K. (2012) Inhibiting Properties of Morpholine as Corrosion Inhibitor for Mild Steel in 2N Sulphuric Acid and Phosphoric Acid Medium. *European Journal of Chemistry*, **9**, 2213-2225. https://doi.org/10.1155/2012/904353

[40] Goulart, C.M., Esteves-Souza, A., Martinez-Huitle, C.A., Rodrigues, C.J.F., Maciel, M.A.M. and Echevarria, A, (2013) Experimental and Theoretical Evaluation of Semicarbazones and Thiosemicarbazones as Organic Corrosion Inhibitors. *Corrosion Science*, **67**, 281-291. https://doi.org/10.1016/j.corsci.2012.10.029

[41] Lasia, A. (2014) Electrochemical Impedance Spectroscopy and Its Applications. Springer, New York. https://doi.org/10.1007/978-1-4614-8933-7

[42] http://www.abc.chemistry.bsu.by/vi/analyser/

[43] Mcquarie, D.A. and Simon, J.D. (1997) Physical Chemistry: A Molecular Approach. University Science Book, California.

[44] Zhao, Y. and Truhlar, D.G. (2008) The M06 Suite of Density Functionals for Main Group Thermochemistry, Thermochemical Kinetics, Noncovalent Interactions, Excited States, and Transition Elements: Two New Functionals and Systematic Testing of Four M06-Class Functionals and 12 Other Functionals. *Theoretical Chemistry Accounts*, **120**, 215-241. https://doi.org/10.1007/s00214-007-0310-x

[45] Adamo, C. and Barone, V. (1999) Toward Reliable Density Functional Methods without Adjustable Parameters: The PBE0 Model. *Journal of Chemical Physics*, **110**, 6158. https://doi.org/10.1063/1.478522

[46] Mennucci, B., Cancès, E. and Tomasi, J. (1997) Evaluation of Solvent Effects in Isotropic and Anisotropic Dielectrics and in Ionic Solutions with a Unified Integral Equation Method: Theoretical Bases, Computational Implementation, and Numerical Applications. *Journal of Physical Chemistry B*, **101**, 10506-10517. https://doi.org/10.1021/jp971959k

[47] Tomasi, J., Mennuci, B. and Cancès, E. (1999) The IEF Version of the PCM Solvation Method: An Overview of a New Method Addressed to Study Molecular Solutes at the QM Ab Initio Level. *Journal of Molecular Structure*: *Teochem*, **464**, 211. https://doi.org/10.1016/S0166-1280(98)00553-3

[48] Frisch, M.J., Trucks, G.W., Schlegel, H.B., Scuseria, G.E., Robb, M.A., Cheeseman, J.R., *et al.* (2013) Gaussian 09, Revision D.01. Gaussian Inc., Wallingford CT.

[49] Panichayupakaranant, P. and Reanmongkol, W. (2002) Evaluation of Chemical Stability and Skin Irritation of Lawsone Methyl Ether in Oral Base. *Pharmaceutical Biology*, **40**, 429-432. https://doi.org/10.1076/phbi.40.6.429.8443

[50] Delarmelina, M., Daltoé, R.D., Cerri, M.F., Madeira, K.P., Rangel, L.B.A., Lacerda Jr., V., Romão, W., Taranto, A.G. and Greco, S.J. (2015) Synthesis, Antitumor Activity and Docking of 2,3-(Substituted)-1,4-Naphthoquinone Derivatives Containing Nitrogen, Oxygen and Sulfur. *Journal of the Brazilian Chemical Society*, **26**, 1804-1816. https://doi.org/10.5935/0103-5053.20150157

[51] Delarmelina, M., Greco, S.J. and Carneiro, J.W.M. (2017) Single Step Mechanism for Nucleophilic Substitution of 2,3-Dichloro Naphthoquinone Using Nitrogen, Oxygen and Sulfur Nucleophiles: A DFT Approach. *Tetrahedron*, **73**, 4363-4370. https://doi.org/10.1016/j.tet.2017.05.095

[52] Venkatesan, A.M., Dehnhardt, C.M., Santos, E.D., Chen, Z., Dos Santos, O., Ayral-Kaloustian, S., Khafizova, G., Brooijmans, N., Mallon, R., Hollander, I., Feldberg, L., Lucas, J., Yu, K., Gibbons, J., Abraham, R.T., Chaudhary, I. and Mansour, T.S. (2010) Bis(Morpholino-1,3,5-Triazine)Derivatives: Potent Adenosine 5'-Triphosphate Competitive Phosphatidylinositol-3-Kinase/Mammalian Target of Rapamycin Inhibitors: Discovery of Compound 26 (PKI-587), a Highly Efficacious Dual Inhibitor. *Journal of Medicinal Chemistry*, **26**, 2636-2645. https://doi.org/10.1021/jm901830p

[53] Carmo, A.M.L., Silva, F.M.C., Machado, P.A., Fontes, A.P.S., Pavan, F.R., Leite, C.Q.F., De A. Leite, S.R., Coimbra, E.S. and Silva, A.D. (2011) Synthesis of 4-Aminoquinoline Analogues and Their Platinum(II) Complexes as New Antileishmanial and Antitubercular Agents. *Biomedicine & Pharmacotherapy*, **65**, 204-209. https://doi.org/10.1016/j.biopha.2011.01.003

[54] Uhlig, H.H. and Revie, R.W. (2008) Corrosion and Corrosion Control: An Introduction to Corrosion Science and Engineering, Wiley Interscience, New Jersey.

[55] Moreira, R.R., Soares, T.F., Gontijo, L.C., Castro, E.V.R. and Ribeiro, J. (2016) Using the Imidazole and Benzimidazole as Corrosion Inhibitor of UNS S31803 Duplex Stainless Steel. *International Journal of Engineering Research & Management Technology*, **03**, 17-21.

[56] Bard, A.J. and Faulkner, L.R. (2001) Electrochemical Methods: Fundamentals and Applications. 2nd Edition, Wiley, New York.

[57] Verma, C., Sorour, A.A., Ebenso, E.E. and Quraishi, M.A. (2018) Inhibition Performance of Three Naphthyridine Derivatives for Mild Steel Corrosion in 1M HCl: Computation and Experimental Analyses. *Results in Physics*, **10**, 504-511. https://doi.org/10.1016/j.rinp.2018.06.054